Far-infrared vibrational properties of linear C$_{60}$ polymers: A comparison between neutral and charged materials

Z.-T. Zhu

Department of Chemistry, State University of New York at Binghamton, Binghamton, New York 13902-6016

J. L. Musfeldt

Department of Chemistry, University of Tennessee, Knoxville, Tennessee 37996

K. Kamarás

Research Institute for Solid State Physics and Optics, Hungarian Academy of Sciences, H-1525 Budapest, Hungary

G. B. Adams and J. B. Page

Department of Physics and Astronomy, Arizona State University, Tempe, Arizona 85287

L. S. Kashevarova, A. V. Rakhmanina, and V. A. Davydov

Institute for High Pressure Physics of the Russian Academy of Science, 142092, Troitsk, Moscow Region, Russian Federation

(Received 25 July 2002; published 29 January 2003)

We report the far-infrared transmittance spectrum of a pure phase of the orthorhombic high-temperature and high-pressure C$_{60}$ polymer and compare the results with a previously published spectrum of the charged RbC$_{60}$ orthorhombic polymer. Assignments for both spectra are made with the aid of first-principles quantum molecular dynamics simulations of the two materials. We find that the striking spectral differences between the neutral and charged linear fullerene polymers can be fully accounted for by charge effects on the C$_{60}$ ball.

I. INTRODUCTION

Among the novel C$_{60}$-based materials, fullerene polymers have attracted a great deal of attention. The polymerization reaction can be carried out using both physical (pressure, temperature, light) and chemical (doping) methods, resulting in neutral and charged polymers, respectively. Under high-temperature and high-pressure (HTHP) conditions, one-dimensional orthorhombic,[1–4] (O) and two-dimensional tetragonal[1,5,6] (T) and rhombohedral[1,7,8] (R) phases have been prepared. In these materials, the fullerene building blocks are connected by four-membered rings, formed via 2+2 cycloaddition.[9,10] Alkali-metal doping can also result in a fullerene polymer.[11–13] Although the spectra of the alkali salts (AC$_{60}$, A = K, Rb, Cs) show a free carrier background above 100 cm^{-1} (Refs. 14 and 15) and the HTHP O polymer is a true insulator, x-ray diffraction confirms that they have similar structures.[3,16,17] Both consist of linear chains of fullerene molecules with D_{2h} on-ball symmetry connected by 2+2 cycloaddition [Fig. 1(a)], but in the AC$_{60}$ O polymer, each ball formally has one excess delocalized negative charge.

The vibrational spectrum of isolated C$_{60}$ exhibits four T_{1u} infrared-active modes and ten Raman-active modes (H_g and A_g), as expected for a cage with icosahedral symmetry.[18,19] The reduced symmetry of the C$_{60}$ balls in the polymerized materials results in a much larger number of infrared- and Raman-active modes.[9,20] In our previous work,[21,22] we assigned the majority of far-infrared spectral features of the neutral two-dimensional polymers with the support of quantum molecular dynamics (QMD) calculations. For the O-polymer material, however, our mode assignments were

not reliable enough to permit a detailed comparison with those of the analogous charged polymer, mainly because of the multiphase nature of the sample, which resulted in a large number of unassigned features and ambiguous mode assignments.

Improvement in sample quality now provides an opportunity to refine the O-polymer mode assignments and then to compare the infrared (IR) spectra of the HTHP and RbC$_{60}$ O polymers. The striking spectral differences raise interesting questions about the effect of negative charge on the vibrational mode character in these materials, an issue that is addressed in this work. In analogy with many of the prototypical organic charge-transfer salts,[23,24] it has also been anticipated that vibronic coupling may influence the dynamics of charged fullerenes.[25–28] Indeed, a recent analysis of IR and Raman data from a number of doped fullerene systems successfully separated charge and vibronic effects on the basis of a simple phenomenological model;[28] however, a quantitative test of the role of vibronic coupling in the multiply bonded fullerene materials has been missing.

In this work, we present far-IR transmittance measurements on a high-quality O-polymer sample, and we compare our results with a previously published RbC$_{60}$ far-IR spectrum.[29] Our comparison is supported by QMD simulations of both materials, allowing us to investigate the influence of charge on the IR spectrum of the linear O polymer. Such an assessment has connotations for the physics of related two-dimensional charged materials such as Na$_4$C$_{60}$, as well as potential utility for understanding heat dissipation in HTHP polymer-based devices that may exploit the novel properties of these materials.[30]
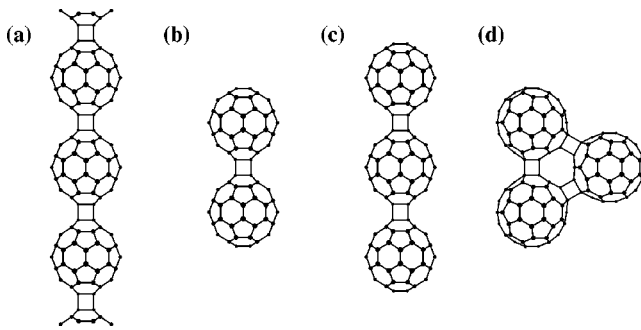
FIG. 1. HTHP *O*-polymer structure (a) and possible "underpolymerized" defect structures (b)–(d).

II. MATERIALS AND METHODS

A. Infrared measurements

All *O*-polymer samples were in the form of black powder. To prepare pellets for our measurements, the materials were crushed, ground with paraffin at 77 K, and compressed under vacuum at 1.5 kbar. The *O*-polymer powder was evenly suspended in the paraffin matrix to form dark brown pellets, suitable for far-IR transmittance measurements. Several different concentrations were required to reveal all features.

Far-IR transmittance measurements were carried out on a Bruker 113V Fourier transform infrared spectrometer equipped with a He-cooled Si bolometer detector. The spectral range 30–650 cm^{-1} was covered with four different beam splitters. The measurements were done at low temperature ($\sim$10 K), achieved with an open-flow cryostat. The spectral resolution is 0.5 cm^{-1}. It is our experience that both low temperature and high resolution are helpful to resolve weak modes and narrow line shapes. All features reported here are reproducible with different concentrations of *O*-polymer–paraffin pellets.

B. Materials

Production of a pure phase of the *O* polymer has been difficult because the preparation conditions for the linear polymer are in a small and somewhat precarious area of the pressure-temperature phase space.[4,8] Samples are routinely contaminated with the *T* polymer and other defect structures. Figure 2 displays the far-IR spectra of three independently prepared samples in the 500–600 cm^{-1} frequency range. Sample 1 was prepared at 1.2 GPa and 573 K for 5.5 h using the temperature-pressure path of Ref. 8. Samples 2 and 3 were prepared at 1.5 GPa and 573 K for 1 h.

Comparing the spectra of the three different *O*-polymer samples, we observe serious tetragonal contamination in sample 3. Tetragonal modes at 363 (not shown), 509, 523 (overlaps with other modes), 533, 555, and 606 cm^{-1}, denoted with a "t" in the lower panel of Fig. 2, are strong, indicating a mixed-phase material. Such a mixed phase of the *O* and *T* polymers is fairly common.[4,20] Features related to *T*-polymer contamination decrease in intensity in sample 2 and are nearly absent in sample 1. Sample 1 clearly has the least *T*-polymer contamination. It also contains the largest amount of unreacted C$_{60}$ monomer, as indicated by the sharp
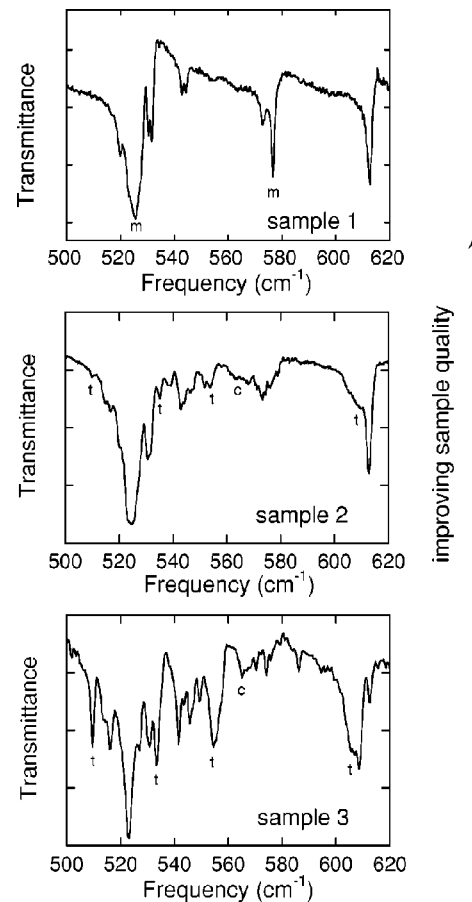

FIG. 2. Comparison of the 10 K transmittance spectra of the three different HTHP *O*-polymer samples in the spectral range from 500 to 620 cm^{-1}. "t" indicates modes of possible tetragonal polymer contamination; "m" denotes likely C$_{60}$ monomer modes; "c" denotes possible chain end modes. The spectrum in the upper panel is of the highest quality sample, whereas that in the lowest panel is poor. That in the middle panel was previously reported and analyzed by Long *et al.* in Ref. 21.

peaks at 526 and 577 cm^{-1}. These two peaks are due to the $T_{1u}(1)$ and $T_{1u}(2)$ modes of I_h C$_{60}$ and are indicated by "m" in the upper panel of Fig. 2.[31] Therefore, we conclude that samples 2 and 3 are both rather "overpolymerized," whereas sample 1 is somewhat "underpolymerized." Nevertheless, of the three spectra, that of sample 1 is superior. It has the simplest and sharpest response, indicating that it corresponds to the highest-quality *O* polymer. Comparison of the same three samples in the 420–500 cm^{-1} frequency range (not shown), where only defect-induced peaks are expected to appear, leads to the same conclusion. In the remainder of this paper, we concentrate our analysis on the highest-quality material (sample 1), which was prepared under optimum and well-studied temperature-pressure conditions.[4]

C. Theoretical methods

Our first-principles simulation technique is quantum molecular dynamics.[32] As described in Ref. 37, this method is

used to calculate the equilibrium geometries and normal modes for all of our simulated structures. The method's major approximations are the local density approximation (LDA), use of a minimal basis set of four confined pseudo-atomic orbitals per atom (sp^3), and use of the non-self-consistent Harris energy functional. The normal modes are evaluated in the harmonic approximation. The method has been successfully applied to fullerene molecules,[33] polymerized fullerenes,[21,22,34–37] and novel carbon solids. For I_h C_{60}, our calculated frequencies are known to be reliable in the frequency range of interest, 200–600 cm^{-1}.[38] We note that, as discussed in Refs. 21, 22, 37, and 38, our first-principles IR strengths are not fully reliable for all modes; hence, we have not used them in making our assignments.

Our relaxed equilibrium geometry for the HTHP O polymer is shown in Fig. 1(a); we will denote this structure as $(C_{60})_n$. We have treated the AC_{60} O polymer as an infinite chain of singly charged C_{60}'s, which we will denote as $(C_{60}^-)_n$. Here, the subscript n denotes the degree of polymerization. In both simulations, we have used one C_{60} ball per unit cell.[39] Although our calculated bond lengths for $(C_{60}^-)_n$ are slightly different than for $(C_{60})_n$ (the biggest difference is less than 1%), to the eye the structure is identical to that of Fig. 1(a). We have also simulated several possible structural defects which may appear in the HTHP O polymer. The most likely ''overpolymerized'' defects include the T polymer and precursors to the full T-polymer planes, such as double chains (two O-polymer chains connected side by side). These structures are shown in Fig. 1 of our earlier work on the T polymer.[22] The most likely ''underpolymerized'' defects are ''chain-end'' defects, i.e., the C_{60} balls which occur at the end of an oligomer.[40] We have simulated two structures which contain these types of C_{60} balls, the dimer of Fig. 1(b) and the linear trimer of Fig. 1(c). In addition, each of these structures is itself a possible ''underpolymerized'' defect in the O polymer. Another likely defect structure is the (equilateral) triangular trimer [Fig. 1(d)]; it has been proposed as the principal component of the C_{60} photopolymer.[36,41]

III. RESULTS AND DISCUSSION

A. Analysis of the HTHP O-polymer spectrum

Figure 3 displays the far-IR spectrum of the O polymer at 10 K. The experimental peak frequencies in Fig. 3 are assigned to IR-active O-polymer vibrational modes based upon a comparison with our QMD calculations. Table I presents our combined experimental and theoretical results. The experimental peak frequencies are in the first column, with the calculated mode frequencies appearing in the second column. The remaining columns contain the symmetry, the quantitative I_h C_{60} ''parent symmetries,'' the polarization, and the percent error for each calculated mode, based upon our selected assignments.[42] The quantitative parent symmetries are obtained by expanding each calculated O-polymer normal-mode eigenvector as a linear combination of the complete set of QMD-calculated mode eigenvectors for I_h C_{60}. With all eigenvectors normalized, the squared expan-
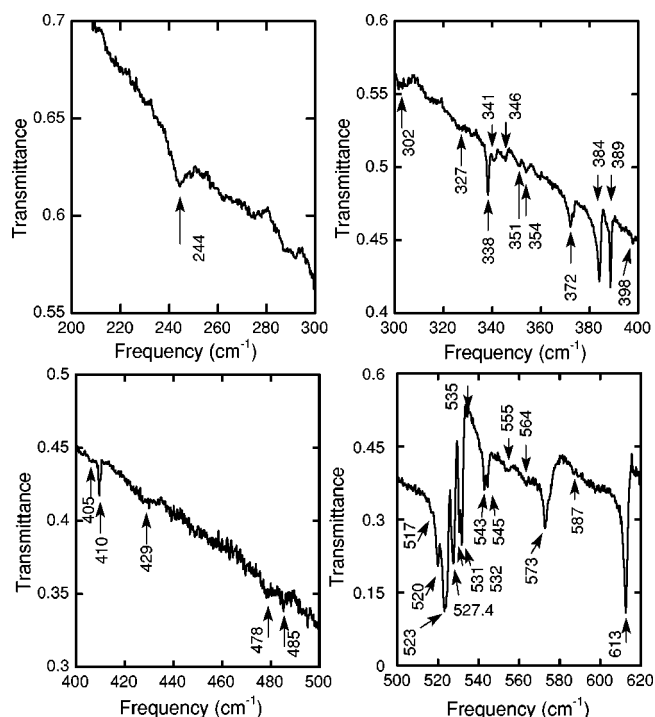

FIG. 3. Transmittance spectrum of the HTHP O polymer at 10 K. Frequencies are labeled for all reproducible modes. Different concentrations of O polymer in the paraffin matrix account for variable background transmittance levels in the different panels. In the lower right-hand panel, the C_{60} monomer modes at 526 and 577 cm^{-1} have been subtracted from the original experimental data.

sion coefficients give the percent contributions of each I_h C_{60} mode to each of the polymer modes. These results show, not surprisingly, that several O-polymer modes derive from more than one I_h C_{60} parent.

Compared with our previous work on the O polymer,[21] we find six newly resolved features. Due to the observation of these new features and the elimination of contamination peaks in the spectrum, 10 of the 18 mode assignments from Ref. 21 are revised. Slight changes in the calculated frequencies are due to the use of a refined (lower-energy) lattice vector in the present work. Also, in our previous publication, parent symmetries were determined qualitatively by a visual identification of I_h C_{60} mode patterns, necessarily resulting in an oversimplified view of polymer-mode parentage. The quantitative parent symmetries (Table I) reveal a more complex mixing of the I_h C_{60} modes in the polymer vibrations.

In the 300–410 cm^{-1} spectral range, newly resolved features at 327, 341, 351, and 354 cm^{-1} are assigned to modes derived primarily from $T_{3u}(1)$ and $G_u(1)$ parent symmetries. Further, features assigned to modes with majority $H_u(1)$ parentage at 384, 389, and 410 cm^{-1} are more well defined than previously reported.[21] The overall splittings of $T_{3u}(1)$-derived, $G_u(1)$-derived, and $H_u(1)$-derived modes are ~45, 16, and 26 cm^{-1}, respectively. Consistent with this substantial mode splitting, features with different I_h parentage overlap. Based on our assignments and the eigenvector analysis, the majority of experimental peaks in the 300–410 cm^{-1} region can be considered as singly derived, since the contribution from a single I_h C_{60} parent is larger than 80% in

TABLE I. Experimental frequencies of the HTHP O polymer, compared with calculated frequencies simulated by first-principles QMD calculations. The site symmetry of the O polymer is D_{2h}. The method of parent symmetry determination is described in the text. For the polarizations, z is in the chain direction, y is normal to the plane of the four-membered rings connecting the balls, and x is in that plane and normal to z.

Frequency (cm^{-1})		Symmetry	Parent symmetries			Polarization	% Error [a]
Experimental	Calculated						
244	-						
302	-						
327	309	B_{1u}	87.5% $T_{3u}(1)$			z	−5.5
338	324	B_{3u}	93.0% $G_u(1)$			x	−4.1
341	330	B_{2u}	93.0% $T_{3u}(1)$			y	−3.2
346	-						
351	348	B_{1u}	78.8% $G_u(1)$			z	−0.9
354	349	B_{2u}	93.7% $G_u(1)$			y	−1.4
372	366	B_{3u}	74.3% $T_{3u}(1)$	14.5% $H_u(1)$		x	−1.6
384	379	B_{1u}	90.7% $H_u(1)$			z	−1.3
389	379	B_{2u}	88.9% $H_u(1)$			y	−2.6
398,405	-						
410	397	B_{3u}	73.4% $H_u(1)$	13.1% $T_{3u}(1)$		x	−3.2
429,478,485	-						
517	-						
520	503	B_{1u}	85.2% $T_{1u}(2)$			z	−3.3
523	516	B_{3u}	43.6% $H_u(2)$	41.0% $T_{1u}(1)$		x	−1.3
526	-		Monomer mode				
527	517	B_{2u}	78.8% $H_u(2)$			y	−1.9
531	521	B_{1u}	87.7% $T_{1u}(1)$			z	−1.9
532	525	B_{2u}	90.4% $T_{1u}(1)$			y	−1.3
535	-						
543	530	B_{3u}	56.1% $T_{1u}(2)$	24.1% $H_u(2)$	10.6% $T_{1u}(1)$	x	−2.4
545	540	B_{2u}	93.4% $T_{1u}(2)$			y	−0.9
555	-						
564	-						
573	551	B_{1u}	86.7% $H_u(2)$			z	−3.8
577	-		Monomer mode				
587	-						
613	595	B_{3u}	37.1% $T_{1u}(2)$	24.7% $T_{1u}(1)$	15.3% $H_u(2)$	x	−2.9
							Average −2.4

[a]Error=[(calc−expt)/expt]×100%.

most cases. Exceptions are the 372 and 410 cm^{-1} structures, which are mixed $H_u(1)$ and $T_{3u}(1)$ modes.

The significantly improved sample quality is particularly evident in the 500–620 cm^{-1} spectral range (Fig. 3). Newly resolved spectral features are observed at 532 and 545 cm^{-1}. According to our assignments, the 531 and 532 cm^{-1} peaks have majority $T_{1u}(1)$ parent symmetry, the 520 and 545 cm^{-1} peaks are largely $T_{1u}(2)$ derived, and the 527 and 573 cm^{-1} features are mainly derived from $H_u(2)$ parent symmetry. Three other modes, at 523, 543, and 613 cm^{-1}, have considerable mixing of $T_{1u}(1)$, $T_{1u}(2)$, and $H_u(2)$ I_h C$_{60}$ parent symmetries. We note that, in our previous work, even greater collective character was found for modes of the two-dimensional T and R polymers;[22] the degree of mode mixing seems to correlate with on-ball distortion. Finally, the feature at 520 cm^{-1} is assigned to a $T_{1u}(2)$-derived mode which is polarized in the stretched direction. The frequency of this

mode is strongly downshifted from the I_h C$_{60}$ T_{1u} frequency of 577 cm^{-1}, lower than that of any mode with a substantial $T_{1u}(1)$ or $H_u(2)$ contribution. This finding is ubiquitous among the HTHP polymers.[21,22]

The unassigned features in the HTHP O-polymer spectrum are small compared with the typical size of the assigned features and are assumed to be due to remaining "overpolymerized" and "underpolymerized" defects in our O-polymer sample. Several of these features are likely to be due to chain-end defects (for example, the weak feature at 564 cm^{-1}), but any detailed assignments at this time would be highly speculative. It is also possible that some of the medium-intensity doublets (531/532 and 543/545) are due to mode splitting, potentially the result of a poorly understood interaction between the O-polymer chains. If this were the case, some of the modes would have to be reassigned to weaker spectral features. Some uncertainty is also unavoid-

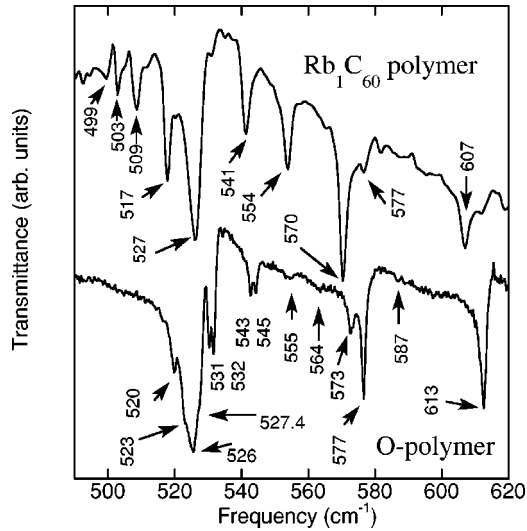FIG. 4. Comparison of the IR transmittance spectra of the HTHP and RbC_{60} O polymers in the spectral range from 490 to 620 cm^{-1}. The spectra are offset for clarity. The RbC_{60} spectrum is from Ref. 29. Note that the T_{1u} C_{60} monomer peaks at 526 and 577 cm^{-1} have not been subtracted from either spectrum.

able because several of the O-polymer modes are close together in frequency; we have assumed that the QMD frequency order matches that of experiment, but other assignments are possible. A polarized experiment on a single-crystal O-polymer sample would be useful to eliminate the remaining uncertainty in the assignments.

B. Comparison between HTHP and RbC_{60} O-polymer spectra

Figure 4 compares a portion of the IR spectrum of the HTHP O polymer with that of the linear charged polymer RbC_{60}. The spectrum of the Rb-doped O polymer is from Ref. 29. In this frequency range, the two spectra display distinct differences. From 560 to 620 cm^{-1}, there are only

two features in each spectrum; these features are similarly spaced. However, between 490 and 560 cm^{-1}, the vibrational features in the HTHP-polymer spectrum are clustered together, in contrast to well-separated peaks in the spectrum of the doped material. Overall, the peaks are much narrower and sharper in the neutral O-polymer spectrum, indicating that the intrinsic damping in this structure is lower than in RbC_{60}. These two materials are known to be nearly isostructural.[3,16,17] Furthermore, the Raman spectra of the neutral and charged O polymers exhibit essentially a one-to-one correspondence between peaks, with only a modest broadening and redshifting of the spectral lines of the charged polymer.[43] Still, the modest broadening and redshifting in the Raman spectrum do leave open the possibility that vibronic coupling may play a small role in the dynamics of RbC_{60}, so the distinct differences in the two IR spectra of Fig. 4 raise interesting questions about the relative importance of charge and vibronic effects.

In an effort to understand the spectral differences between the HTHP and RbC_{60} O polymers, we have used QMD to calculate the IR spectra for both $(C_{60})_n$ and $(C_{60}^-)_n$.[44] Our results are displayed in Tables I and II and in Fig. 5. For our comparison of the IR spectra of the HTHP and RbC_{60} O polymers, the frequency region of interest is 490–620 cm^{-1}; each polymer has nine calculated modes in this range. Of these nine features, the two highest-frequency modes are found to be similarly spaced, in agreement with experiment. For the seven lower-frequency modes, those of $(C_{60}^-)_n$ are well separated compared to the features of $(C_{60})_n$, also in agreement with experiment (Fig. 4). Specifically, the calculated HTHP frequencies for these seven modes have four separations of less than 6 cm^{-1}, whereas the calculated RbC_{60} frequencies of these seven modes have only one such separation. Thus, adding charge significantly reorganizes and "spreads out" the modes between 490 and 620 cm^{-1}.

Our assignments for the far-IR vibrational features of the Rb-doped C_{60} polymer are presented in Table II. The average

TABLE II. Experimental frequencies of the Rb-doped O polymer, compared with calculated frequencies simulated by first-principles QMD calculations. For the polarizations, z is in the chain direction, y is normal to the plane of the four-member rings connecting the balls, and x is in that plane and normal to z.

Frequency (cm^{-1})		Symmetry	Parent symmetries			Polarization	% Error [a]
Experimental	Calculated						
499	500	B_{1u}	57.6% $T_{1u}(1)$	39.1% $T_{1u}(2)$		z	+0.2
509	506	B_{2u}	82.4% $H_u(2)$			y	−0.6
-	513	B_{1u}	51.1% $T_{1u}(2)$	35.9% $T_{1u}(1)$		z	
519	516	B_{3u}	41.6% $H_u(2)$	39.9% $T_{1u}(1)$		x	−0.6
526	-		Monomer mode				
527	526	B_{2u}	92.8% $T_{1u}(1)$			y	−0.2
542	534	B_{3u}	57.2% $T_{1u}(2)$	32.1% $H_u(2)$		x	−1.5
555	542	B_{2u}	91.9% $T_{1u}(2)$			y	−2.3
571	551	B_{1u}	83.4% $H_u(2)$			z	−3.5
577	-		Monomer mode				
608	591	B_{3u}	33.4% $T_{1u}(2)$	28.0% $T_{1u}(1)$	14.6% $H_u(2)$	x	−2.8
-						Average	−1.4

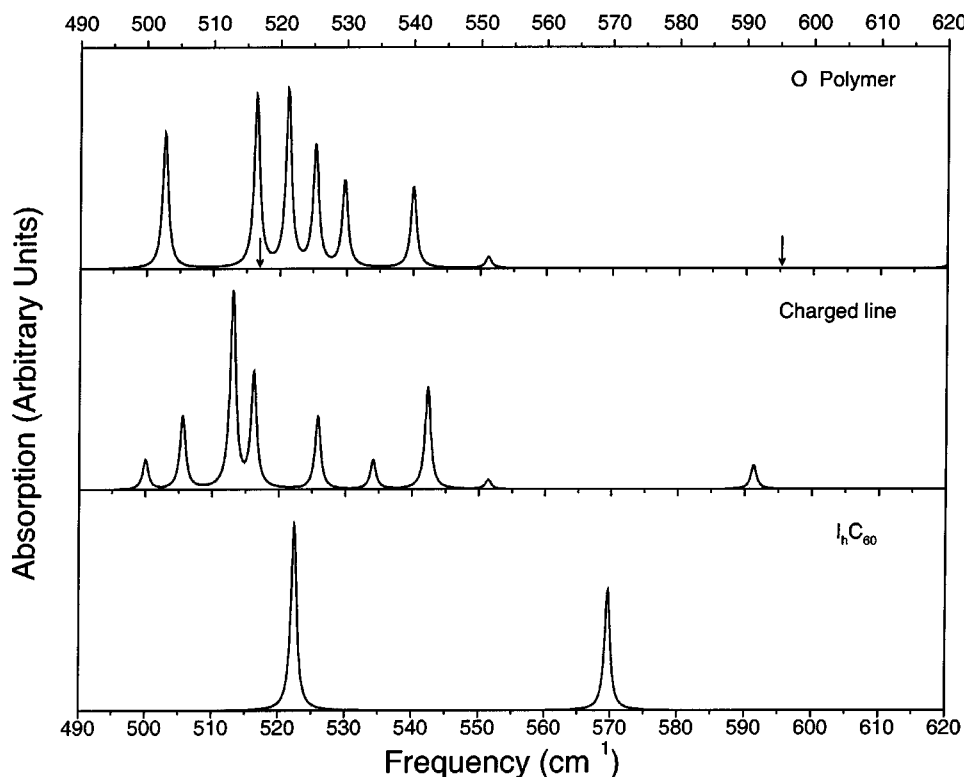[a]Error = [(calc−expt)/expt]×100%

FIG. 5. Calculated IR spectra of the HTHP O polymer, the RbC_{60} O polymer, and the I_h C_{60} monomer in the frequency range 490–620 cm^{-1}. These calculated spectra have been broadened with small linewidth Lorentzians. There is no relation between the calculated mode intensities in the different panels. The arrows in the O-polymer panel at ~517 and 595 cm^{-1} indicate the locations of peaks which are too small to be seen on this scale; their integrated intensities are about seven and 150 times smaller, respectively, than the integrated intensity of the 551 cm^{-1} peak. As noted in the text, our calculated strengths have not been used in making the assignments presented in Tables I and II.

error between the experimental frequencies and the calculated frequencies of the assigned modes is ~1.5%, slightly less than for the HTHP O polymer. The quantitative parent symmetries, along with the calculated polarization directions, provide a detailed description of the calculated mode patterns and allow for a direct comparison of the $(C_{60})_n$ and $(C_{60}^-)_n$ vibrations. For both polymers, the nine modes in the frequency range of interest are found to be primarily derived from the $T_{1u}(1)$, $T_{1u}(2)$, and $H_u(2)$ I_h C_{60} parent vibrations. Of these nine modes, the parentage of the two higher-frequency features is quite similar for both polymers; however, only five of the seven lower-frequency modes have

similar parentage. The z-polarized $T_{1u}(1)$- and $T_{1u}(2)$-derived modes of $(C_{60})_n$ (at calculated frequencies of 521 and 503 cm^{-1}) are almost equally mixed in $(C_{60}^-)_n$ to create two new modes of quite different character (at calculated frequencies of 500 and 513 cm^{-1}). In comparing the assigned frequencies of the HTHP and RbC_{60} O polymers for the purpose of assessing the probable strength of vibronic coupling, we will compare only the frequencies of the seven modes which are found to have similar parentage.

Table III presents a detailed comparison between the IR-active modes of the HTHP and doped O polymers. The first column identifies the mode symmetry and primary I_h parent-

TABLE III. Comparison of the infrared features of HTHP and RbC_{60} O polymers between 490 and 620 cm^{-1}. $(C_{60})_n$ and $(C_{60}^-)_n$ indicate the HTHP and RbC_{60} O polymers, respectively. All frequencies are in cm^{-1}. Note that the two modes of B_{1u} symmetry are omitted from this table, as our predictions for mode character changes substantially between neutral and charged polymers, making such a comparison invalid. In $(C_{60})_n$, the calculated 503 and 521 cm^{-1} modes are $T_{1u}(2)$ and $T_{1u}(1)$ derived, whereas in $(C_{60}^-)_n$, these modes are mixed. Δ_{calc} = calculated frequency of $(C_{60}^-)_n$ − calculated frequency of $(C_{60})_n$; Δ_{expt} = experimental frequency of $(C_{60}^-)_n$ − experimental frequency of $(C_{60})_n$.

Mode symmetry	Calculated frequency			Experimental frequency			$\Delta_{expt} - \Delta_{calc}$
	$(C_{60})_n$	$(C_{60}^-)_n$	Δ_{calc}	$(C_{60})_n$	$(C_{60}^-)_n$	Δ_{expt}	
B_{3u} $[\to H_u(2)]$	516 [a]	516 [a]	0	523	519	−4	−4
B_{2u} $[\to H_u(2)]$	517	506	−11	527	509	−18	−7
B_{2u} $[\to T_{1u}(1)]$	525	526	+1	532	527	−5	−6
B_{3u} $[\to T_{1u}(2)]$	530 [a]	534 [a]	+4	543	542	−1	−5
B_{2u} $[\to T_{1u}(2)]$	540	542	+2	545	555	+10	+8
B_{1u} $[\to H_u(2)]$	551	551	0	573	571	−2	−2
B_{3u} $[\to T_{1u}(2)]$	595 [a]	591 [a]	−4	613	608	−5	−1

[a]Indicates a mixed mode.

age. The second column presents the calculated frequencies for the two simulations and the calculated frequency shift Δ_{calc} between charged and neutral species. Similar information is listed for the experimental vibrational features in the third column. The last column compares the experimental to the calculated frequency shifts between charged and neutral species. All values of $\Delta_{expt} - \Delta_{calc}$ are small, well within the typical 3% error of our QMD calculations in this frequency range. The good correspondence between calculated and experimental frequency shifts for the HTHP and doped O polymers suggests that the differences in the observed IR spectra (Fig. 4) result primarily from the charge-induced distortion of the C_{60} cage.[45] This conclusion is consistent with a recent scaled quantum mechanical calculation for the vibrational modes of C_{60} and C_{60}^{6-} by Choi *et al.*,[46] which indicates that the effect on C_{60}^{6-} is largely due to bond equalization in the charged fullerene. Hence we conclude that the observed far-IR differences between the orthorhombic HTHP polymer and RbC_{60} are mainly related to the charge-induced distortion of the C_{60} balls. Any vibronic coupling would thus be small.

An independent method of assessing the role of vibronic coupling in the IR response of O-polymerized RbC_{60} is to consider the symmetry of the seven modes listed in Table III. Previous attempts to assess the vibronic coupling of charged C_{60}'s have neglected this aspect by assuming that the T_{1u} modes retain their character in the charged material.[28,47]

In the "charged-phonon" model proposed by Rice and Choi,[47] the novel behavior of the T_{1u} modes for C_{60}^{n-} molecules was explained in terms of the coupling of intramolecular vibrations to the $t_{1u} \rightarrow t_{1g}$ electronic excitations involving the single-particle orbitals. The IR intensity is predicted to increase quadratically with charge, and the mode frequencies are predicted to decrease linearly with charge. Subsequent work showed that both predictions of the charged-phonon model are oversimplified for the C_{60}^{n-} system.[28,48] In Ref. 28, Hands *et al.* studied the separation of vibronic coupling and charge effects for a variety of doped fullerenes by means of a phenomenological model. Within this framework, vibronic effects were evaluated from a large set of literature data over a wide range of charge by assuming that the total frequency shift of a mode from its value in the neutral material is the sum of charge-transfer and vibronic terms; monoanionic species received particular attention. In the more complicated materials, the authors neglected symmetry lowering arising from polymerization, a consideration that is important for certain compounds in their large data set. Our understanding of mode constituencies in the neutral and charged O polymers therefore provides an opportunity to extend this analysis of vibronic coupling to multiply bonded fullerenes, where the on-ball symmetry is lowered due to the polymerization. For the case of $(C_{60}^{-})_n$, we do not expect spectacular frequency shifts, even if a vibronic coupling mechanism is present, because only one charge has been added to the fullerene ball (see Fig. 3 of Ref.

28). Nevertheless, if the vibronic coupling constant λ is ~ 0.1, a 2% frequency shift might be expected in this case.[28] In the frequency range of interest here, this corresponds to $\sim 10 \, \text{cm}^{-1}$, which ought to be discernible in our experiments.

For the O polymer, reasonably strong coupling should cause broadening and softening of some modes,[49] but due to the on-ball distortion in the polymer, the symmetry of both electronic orbitals and intramolecular vibrations will be different from icosahedral C_{60}, leading to modified selection rules. The lowest unoccupied molecular orbital (LUMO), in this case, is of b_{1u} symmetry, and excitations can occur for the t_{1g}-derived b_{1g}, b_{2g}, and b_{3g} levels. In the D_{2h} group, $b_{1u} \otimes b_{1g} = A_u$, $b_{1u} \otimes b_{2g} = B_{3u}$, and $b_{1u} \otimes b_{3g} = B_{2u}$. Therefore, the IR modes with B_{2u} and B_{3u} symmetry should be affected by the coupling, whereas those with B_{1u} character should not. Table III does not show any significantly different behavior for the single B_{1u} mode, as compared to modes of the other two symmetries. We regard this insensitivity as additional proof for weak, if any, vibronic coupling in the linear charged polymer $[(C_{60}^{-})_n]$. It should be noted that in other fulleride systems, some modes shift dramatically while others shift very little.[28] Thus, it may be useful to extend this analysis to other, more highly charged, fullerene polymer systems.

IV. CONCLUSION

We have measured the far-IR vibrational properties of a pure phase of the HTHP orthorhombic C_{60} polymer. Modes were assigned with the aid of our quantum molecular dynamics calculations, and parent symmetries were determined by eigenvector analysis. Despite the observed mixing, there are far fewer collective modes in the O polymer compared to the previously studied two-dimensional T and R polymers.[21,22] We attribute this difference to a smaller on-ball distortion in the O polymer compared to the other materials. The striking differences between the IR response of the neutral and the previously published spectrum of charged O polymer[29] were discussed and analyzed. The variation in IR properties over the $490-620 \, \text{cm}^{-1}$ range can be accounted for by charge effects on the C_{60} ball. According to our analysis, vibronic coupling is weak in the linear charged polymer.

[1] M. Núñez-Regueiro, L. Marques, J.-L. Hodeau, O. Béthoux, and M. Perroux, Phys. Rev. Lett. **74**, 278 (1995); Phys. Rev. B **57**, 5543(E) (1998).

[2] V. Agafonov, V. A. Davydov, L. S. Kashevarova, A. V. Rakhmanina, A. Kahn-Harari, P. Dubois, R. Ceolin, and H. Szwarc, Chem. Phys. Lett. **267**, 193 (1997).

[3] R. Moret, P. Launois, P.-A. Persson, and B. Sundqvist, Europhys. Lett. **40**, 55 (1997).

[4] V. A. Davydov, L. S. Kashevarova, A. V. Rakhmanina, V. Agafonov, H. Allouchi, R. Céolin, A. V. Dzyabchenko V. M. Senyavin, H. Szwarc, T. Tanaka, and K. Komatsu, J. Phys. Chem. B **103**, 1800 (1999).

[5] V. A. Davydov, L. S. Kashevarova, A. V. Rakhmanina, V. Agafonov, H. Allouchi, R. Céolin, A. V. Dzyabchenko, V. M. Senyavin, and H. Szwarc, Phys. Rev. B **58**, 14 786 (1998).

[6] R. Moret, P. Launois, T. Wagberg, and B. Sundqvist, Eur. Phys. J. B **15**, 253 (2000).

[7] Y. Iwasa, T. Arima, R. M. Fleming, T. Siegrist O. Zhou, R. C. Haddon, L. J. Rothberg, K. B. Lyons, H. L. Carter, Jr., A. F. Hebard, R. Tycko, G. Dabbagh, J. J. Krajewski, G. A. Thomas, and T. Yagi, Science **259**, 955 (1994).

[8] V. A. Davydov, L. S. Kashevarova, A. V. Rakhmanina, V. M. Senyavin, R. Céolin, H. Szwarc, H. Allouchi, and V. Agafonov, Phys. Rev. B **61**, 11 936 (2000).

[9] A. M. Rao, P. Zhou, K. An Wang, G. T. Hager, J. M. Holden, Y. Wang, W.-T. Lee, X.-X. Bi, P. C. Eklund, D. S. Cornett, M. A. Duncan, and I. J. Amster, Science **259**, 955 (1993).

[10] Each four-membered ring consists of two atom-atom connections between balls.

[11] P. W. Stephens, G. Bortel, G. Faigel, M. Tegze, A. Jánossy, S. Pekker, G. Oszlányi, and L. Forró, Nature (London) **370**, 636 (1994).

[12] S. Pekker, A. Jánossy, L. Mihaly, O. Chauvet, M. Carrard, and L. Forró, Science **265**, 1077 (1994).

[13] M. C. Martin, D. Koller, A. Rosenberg, C. Kendziora, and L. Mihaly, Phys. Rev. B **51**, 3210 (1995).

[14] F. Bommeli, L. Degiorgi, P. Wachter, Ö. Legeza, A. Jánossy, G. Oszlanyi, O. Chauvet, and L. Forro, Phys. Rev. B **51**, 14 794 (1995).

[15] O. Chauvet, G. Oszlanyi, L. Forró, P. W. Stephens, M. Tegze, G. Faigel, and A. Jánossy, Phys. Rev. Lett. **72**, 2721 (1994).

[16] P. Launois, R. Moret, J. Hone, and A. Zettl, Phys. Rev. Lett. **81**, 4420 (1998).

[17] B. Renker, H. Schober, R. Heid, and P. V. Stein, Solid State Commun. **104**, 527 (1997).

[18] M. S. Dresselhaus, G. Dresselhaus, and P. C. Eklund, *Science of Fullerenes and Carbon Nanotubes* (Academic Press, New York, 1996).

[19] H. Kuzmany, R. Winkler, and T. Pichler, J. Phys.: Condens. Matter **7**, 6601 (1995).

[20] A. M. Rao, P. C. Eklund, J.-L. Hodeau, L. Marques, and M. Núñez-Regueiro, Phys. Rev. B **55**, 4766 (1997).

[21] V. C. Long, J. L. Musfeldt, K. Kamarás, G. B. Adams, J. B. Page, Y. Iwasa, and W. E. Mayo, Phys. Rev. B **61**, 13 191 (2000).

[22] Z.-T. Zhu, J. L. Musfeldt, K. Kamarás, G. B. Adams, J. B. Page, V. A. Davydov, L. S. Kashevarova, and A. V. Rakhmanina, Phys. Rev. B **65**, 085413 (2002).

[23] M. J. Rice, V. M. Yartsev, and C. S. Jacobsen, Phys. Rev. B **21**, 3437 (1980).

[24] J. E. Eldridge, C. C. Homes, J. M. Williams, A. N. Kini, and H. H. Wang, Spectrochim. Acta, Part A **51(6)**, 947 (1995).

[25] K. Kamarás, D. B. Tanner, and L. Forró, Fullerene Sci. Technol. **5**, 465 (1997).

[26] M. C. Martin, D. Koller, and L. Mihaly, Phys. Rev. B **47**, 14 607 (1993); **50**, 6538 (1994).

[27] T. Pichler, R. Winkler, and H. Kuzmany, Phys. Rev. B **49**, 15 879 (1994).

[28] I. D. Hands, J. L. Dunn, and C. A. Bates, Phys. Rev. B **63**, 245414 (2001).

[29] K. Kamarás, S. Pekker, L. Forró, and D. B. Tanner, Chem. Phys. Lett. **295**, 279 (1998).

[30] T. L. Makarova, B. Sundqvist, R. Hohnes, P. Esquinazi, Y. Kopelevich, P. Scharff, V. A. Davydov, L. S. Kashevarova, and A. V. Rakhmanina, Nature (London) **413**, 716 (2001).

[31] The unreacted T_{1u} C_{60} monomer modes (at 1183 and 1429 cm^{-1}) were also observed in the middle-infrared spectrum of sample 1 in KBr pellet.

[32] O. F. Sankey and D. J. Niklewski, Phys. Rev. B **40**, 3979 (1989).

[33] G. B. Adams, J. B. Page, O. F. Sankey, K. Sinha, J. Menéndez, and D. R. Huffman, Phys. Rev. B **44**, 4052 (1991); G. B. Adams, O. F. Sankey, J. B. Page, M. O'Keeffe, and D. A. Drabold, Science **256**, 1792 (1992).

[34] G. B. Adams, J. B. Page, M. O'Keeffe, and O. F. Sankey, Chem. Phys. Lett. **228**, 485 (1994); J. R. Fox, G. P. Lopinski, J. S. Lannin, G. B. Adams, J. B. Page, and J. E. Fischer, Chem. Phys. Lett. **249**, 195 (1996).

[35] G. B. Adams, J. B. Page, O. F. Sankey, and M. O'Keeffe, Phys. Rev. B **50**, 17 471 (1994).

[36] G. B. Adams and J. B. Page, Phys. Status Solidi B **226**, 95 (2001).

[37] G. B. Adams and J. B. Page, in *Fullerene Polymers and Fullerene-Polymer Composites*, edited by P. C. Eklund and A. M. Rao (Springer-Verlag, Berlin, 2000), p. 185.

[38] J. Menéndez and J.B. Page, in *Light Scattering in Solids, VIII*, edited by M. Cardona and G. Güntherodt (Springer, Heidelberg, 2000), p. 27.

[39] We also employ two special k points in the one-dimensional Brillouin zone.

[40] Note that chain ends are intrinsic features of the linear O polymer and can therefore never be entirely eliminated, even in long chains.

[41] T. Pusztai, G. Oszlányi, G. Faigel, K. Kamarás, L. Gránásy, and S. Pekker, Solid State Commun. **111**, 595 (1999).

[42] The percent error is calculated as error$=[(calc-expt)/expt] \times 100$. Typical differences between theoretical and experimental frequencies are on the order of 3% (Refs. 21 and 22).

[43] J. Winter, H. Kuzmany, S. Soldatov, P.-A. Persson, P. Jacobsson, and B. Sundqvist, Phys. Rev. B **54**, 17 486 (1996).

[44] Infrared strengths are calculated in the linear dipole-moment approximation. Details of the method are available in Ref. 21 and references therein.

[45] Of course errors are possible in our assignments, with higher uncertainty for the HTHP-polymer assignments. Other sets of assignments would change the results in Table III, but for all reasonable sets of assignments the experimental frequency shifts Δ_{expt} would be small; the greatest downshifts would be less than 20 cm^{-1} with the majority of the downshifts less than 10 cm^{-1}. Our fundamental conclusions would not be altered.

[46] C. H. Choi, M. Kertesz, and L. Mihaly, J. Phys. Chem. A **104**, 102 (2000).

[47] M. J. Rice and H.-Y. Choi, Phys. Rev. B **45**, 10 173 (1992).

[48] A. P. Smith and G. F. Bertsch, Phys. Rev. B **53**, 7002 (1996).

[49] The mixed nature of the vibrational modes in the O polymers means that the results of Fig. 4 and Table III cannot be compared directly with the data compiled in Ref. 28, since that compilation assumes that the character of T_{1u} and T_{2u} modes remains essentially unchanged in the singly doped materials.